ADVANCED ENGINEERING MATERIALS
www.aem-journal.com

Microwave-Assisted Synthesis of ZnO Nanoparticles: Phase Transfer to Water

*Patrick E. J. Saloga, Tina Rybak, and Andreas F. Thünemann**

Herein, a simple one-pot procedure is reported to obtain aqueous zinc oxide (ZnO) nanoparticle dispersions from ZnO nanoparticles dispersed in cyclohexane. In the process, polyoxyethylene (20) sorbitan monooleate (polysorbate 80, Tween 80) functions as a phase transfer agent and colloidal stabilizer. The particles grow in a defined manner during the transfer, presumably via coalescence. The final particle radii are tuneable in the range from 2.3 ± 0.1 nm to 5.7 ± 0.1 nm depending on the incubation time of the dispersion at 90 °C. Small-angle X-ray scattering is employed to determine the particle radius distributions before and after phase transfer. The larger ZnO particle radii are associated with a redshift of the optical bandgap and luminescence emission, as expected for semiconductor nanoparticles. The particles presented here exhibit a relative size distribution width of 20%, rendering them attractive for applications in, e.g., biology or catalysis. The latter application is demonstrated at the photocatalytic degradation of methylene blue dye.

1. Introduction

Zinc oxide (ZnO) nanoparticles with defined sizes are of scientific and industrial interest.[1] They are a robust alternative candidate to TiO_2 for cleaning of wastewater.[2,3] Also, photocatalytically active pavings may alternatively be manufactured with ZnO instead of TiO_2, mainly for the degradation of NO_x compounds from combustion engines.[4] Nanoparticles are generally advantageous for catalytic applications, compared to microparticles, as the specific surface area scales reciprocally with particle size. We recently reported a microwave-assisted synthesis of ultrasmall ZnO particles, which are stable long term in cyclohexane.[5] However, depending on the photocatalysis requirements, these particles may need to be available as dispersions in water. Therefore, this study aims to utilize the ZnO nanoparticles, from our previous study, as starting material and provides an easy method to transfer them from cyclohexane to water. Numerous phase transfer reactions are reported in the literature. Among these, the method of Wang et al.[6] is a generic method, which utilizes cyclodextrin as a phase transfer agent. In contrast to that method, the method of the present study produces no remaining organic solvent after phase transfer. The catalytic properties of the resulting aqueous ZnO dispersion have also been tested for the photocatalytic degradation of methylene blue (MB) as a typical model reaction for the degradation of an organic pollutant.[7] Syed et al. reported on a strategy for extraction of ZnO particles from a synthesis medium to a device processing medium using undecanal as a particle receiving liquid and a phase transfer vehicle.[8] Particle extraction through liquid–liquid interface for colloidal processing of ZnO particles was also performed with the use of octanohydroxamic acid and bufexamac as extractors.[9] Lenaerts et al.[10] found that a polar-to-nonpolar solvent phase transfer of TiO_2 and WO_3 nanoparticles could be achieved by using oleylamine, but not dodecane-1-thiol, whereas the opposite holds for ZnO and CuO. In contrast to most phase transfer agents in use, polysorbate 80 is a synthetic nonionic surfactant of highly proven safety, which makes it useful for drug formulation.[11] Therefore, the use of this transfer agent appears to be of interest for possible further uses of the ZnO particles.

2. Results and Discussion

The preparation of water-dispersed ZnO nanoparticles, as presented here, utilizes spherical oleate-stabilized ZnO nanoparticles as starting material. These were prepared in a microwave-assisted synthesis, as previously reported.[5] Briefly, ZnO nanoparticles were synthesized within 5 min in a microwave at 125 °C and obtained as a colloidally stable dispersion in cyclohexane. In the following, we refer to these particles as P_0. The phase transfer to aqueous solution started by the addition of polysorbate 80 (polyoxyethylene (20) sorbitan monooleate, trade name Tween 80) to P_0 yielding particles P_{0+TW}. Water was added next, followed by heating of the samples to 90 °C for 240 min, whereby the cyclohexane was removed completely. This procedure yielded the aqueous ZnO particle dispersion H_{240}. Similarly, Ren et al. have shown that this method is

P. E. J. Saloga, T. Rybak, A. F. Thünemann
6.5 Polymers in Life Science and Nanotechnology
Bundesanstalt für Materialforschung und -prüfung (BAM)
Unter den Eichen 87, 12205 Berlin, Germany
E-mail: andreas.thuenemann@bam.de

P. E. J. Saloga
Fachbereich Biologie, Chemie, Pharmazie
Freie Universität Berlin
Takustraße 3, 14195 Berlin, Germany

The ORCID identification number(s) for the author(s) of this article can be found under https://doi.org/10.1002/adem.202101276.

© 2021 The Authors. Advanced Engineering Materials published by Wiley-VCH GmbH. This is an open access article under the terms of the Creative Commons Attribution License, which permits use, distribution and reproduction in any medium, provided the original work is properly cited.

DOI: 10.1002/adem.202101276

applicable for the upconversion of oleate-stabilized $NaYF_4$:Yb,Er-nanoparticles.[12] Polysorbate 80 is a biocompatible nonionic surfactant, bearing an ethoxylated sorbitan and an oleate chain. The latter was expected to interact with the oleate-coating on the as-synthesized particles, with the hydrophilic groups enabling particle dispersion in water. Besides H_{240}, we were also interested in the intermediate stages of phase transfer. Therefore, samples were additionally taken at heating times of 0, 15, 30, 60, and 90 min. The remaining cyclohexane in these samples was removed at reduced pressure at 40 °C, yielding samples H_0, H_{15}, H_{30}, H_{60}, and H_{90}, respectively.

2.1. Particle Structure

All samples were analyzed with small-angle X-ray scattering (SAXS), and the resulting scattering curves are shown in **Figure 1**. It can be seen that the shape of the curves is characteristic of noninteracting nanoparticles. While SAXS is an accurate

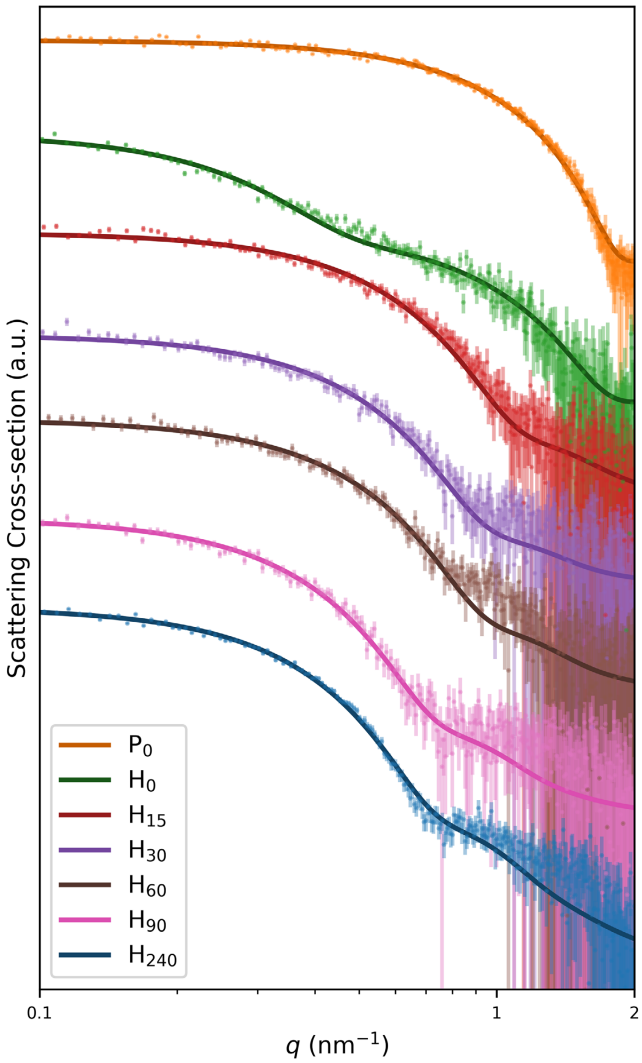

Figure 1. SAXS data (points with error bars) and curve fits (solid lines) of particles in cyclohexane (top curve, before transfer) and aqueous particle dispersions obtained at the denoted heating times (lower curves, heating time increasing toward the bottom). Curves are shifted vertically for better visibility.

method for determining size distributions of particles smaller than 10 nm,[13] the particle shape needs to be known for a detailed SAXS data analysis. Scanning transmission electron microscopy was used for this purpose and confirmed the presence of spherical particles after phase transfer in sample H_{240}, with 90% of the particles in the size range of 5.5 and 8.5 nm (see Figure S1, Supporting Information). As proven earlier, the particles P_0 are also spherical, but much smaller in radii in the range of 2–4 nm.[5] Therefore, we conclude that the particles grow during the phase transfer, but keep their spherical shape. The simplest model for interpretation of the SAXS curves of P_0, P_{0+TW}, H_{15}, H_{30}, H_{60}, H_{90}, and H_{240} is a monomodal log-normal radial distribution of spherical ZnO particles. This simple model was not sufficient for the curve of H_0 for which a bimodal log-normal distribution was found suitable. The resulting curve fits are provided as solid lines in Figure 1.

As for nanoparticles with a ZnO core and a stabilizer shell, the question arises whether the determined radii distributions refer to the cores only or are inclusive of the particle shell. To answer this question, the scattering length densities of ZnO and polysorbate 80 need to be considered. More precisely, for Cu Kα radiation with an energy of 8.04 keV, the scattering length density difference between ZnO and water is $\Delta SLD \simeq 3.31 \times 10^{11}\,cm^{-2}$ and that of polysorbate 80 is $\Delta SLD \simeq 4.39 \times 10^{9}\,cm^{-2}$.[14] Therefore, ZnO scatters 75 times more than the stabilizer, and the scattering of the polysorbate can be neglected in SAXS analysis. In conclusion, it can be stated that SAXS detects the ZnO cores of the particles exclusively.

The mean radii of the ZnO particles before phase transfer in cyclohexane without (P_0) and with added polysorbate 80 (P_{0+TW}) both were $R_{mean} = 2.3 \pm 0.1$ nm and displayed a size distribution width of $\sigma = 0.3 \pm 0.1$ nm (relative width of $\sigma_{rel} = 13 \pm 1\%$). The particles exhibited a mean volume of $\langle V \rangle = 54 \pm 1\,nm^3$ and contained a number of ZnO moieties of $n_{ZnO} = 2250 \pm 40$ when assuming a density of $5.61\,g\,cm^{-3}$. Upon stabilizer addition, there is no change in the size distribution parameters, and thus no influence of the stabilizer on the ZnO cores was detected.

After complete phase transition, in sample H_{240}, values of $R_{mean} = 5.7 \pm 0.1$ nm and $\sigma = 1.2 \pm 0.1$ nm ($\sigma_{rel} = 20\%$) were determined. This corresponds to $<V> = 870 \pm 9\,nm^3$ and $n_{ZnO} = 36\,100 \pm 400$. While the mean volume of H_{240} is larger than that of P_0 by a factor of $n_p = 16$, the relative size distribution width increased only slightly. The value of n_p could be interpreted as meaning that one H_{240} particle was formed from the material of 16 P_0 particles. To gain further insight into the growth mechanism, the particle properties of the intermediate steps of the phase transfer, as shown in **Table 1**, were examined in more detail. The two particle populations of H_0 displayed mean radii of $R_{mean,1} = 2.3 \pm 0.1$ nm and $R_{mean,2} = 7.2 \pm 0.1$ nm. At later stages of the phase transfer, the particle population was monomodal and R_{mean} increased with increasing incubation time in the line of 3.7 nm (H_{15}), 4.3 nm (H_{30}), 4.4 nm (H_{60}), and 5.6 nm (H_{90}) to the final value of 5.7 nm (H_{240}). σ_{rel} was kept constant at 20%, and therefore the σ values increased accordingly.

The observed ZnO particle growth could be explained along the interpretation scheme suggested by Caetano et al. for the formation of ZnO quantum dots.[15] Therein, the initial steps of particle growth result from oriented attachment between several particles, with subsequent coalescence to larger particles. While the low

© 2021 The Authors. Advanced Engineering Materials published by Wiley-VCH GmbH

Table 1. Particle size evolution during phase transfer for primary particles P_0 and phase-transferred particles H_i, obtained after heating to 90 °C for i minutes: listed are mean particle radius R_{mean}, absolute (σ) and relative (σ_{rel}) size distribution widths from SAXS, average particle volume $\langle V \rangle$, the calculative number of primary particles contained therein, n_P, and the calculative number of formula units of ZnO within a particle, n_{ZnO}.

Sample	R_{mean} [nm]	σ [nm]	σ_{rel} (%)	$\langle V \rangle$ (nm^3)	n_P	n_{ZnO}
ZnO Nanoparticles before Phase Transfer in Cyclohexane						
P_0	2.3 ± 0.1	0.3 ± 0.1	13 ± 1	54 ± 1	1	2250 ± 40
P_{0+TW}	2.3 ± 0.1	0.3 ± 0.1	13 ± 1	54 ± 1	1	2250 ± 40
ZnO Nanoparticles after Phase Transfer in Water						
H_0	2.3	0.3	13	54	1	2250
	7.2 ± 0.1	1.5 ± 0.1	20	1770 ± 60	33 ± 2	$74\,000 \pm 3000$
H_{15}	3.7 ± 0.1	0.8 ± 0.1	20	236 ± 5	4 ± 1	9800 ± 200
H_{30}	4.3 ± 0.1	0.9 ± 0.1	20	373 ± 10	7 ± 1	$15\,500 \pm 400$
H_{60}	4.4 ± 0.1	0.9 ± 0.1	20	396 ± 9	7 ± 1	$16\,400 \pm 400$
H_{90}	5.6 ± 0.1	1.2 ± 0.1	20	848 ± 20	16 ± 1	$35\,200 \pm 900$
H_{240}	5.7 ± 0.1	1.2 ± 0.1	20	870 ± 9	16 ± 1	$36\,100 \pm 400$

solubility of ZnO in water could, in principle, enable Ostwald ripening, the aforementioned study showed that the particle growth occurred mainly via aggregation and coalescence.[15] This model could explain the bimodality of the particle radii distribution found for H_0 in which single particles with $R_{mean,1}$ and agglomerated particles with $R_{mean,2}$ were present in parallel. Then, further coalescence would yield larger particles in samples H_{15}, H_{30}, and H_{60}, with n_P values of 4–7, and then proceed to samples H_{90} and H_{240}, with $n_P = 16$, respectively.

Dynamic light scattering (DLS) was employed to determine the hydrodynamic radii of the particles, which were in the range of about 4–8 nm, but without apparent differences between the different particles. Very likely, the presence of the polymeric surfactant, which itself forms micelles with radii of around $R_h = 4$ nm,[16] prevents a more precise determination of the hydrodynamic radii. Nevertheless, the hydrodynamic radii represent the total particle, including its stabilizing shell, and when comparing the hydrodynamic radii with the ZnO core radii from SAXS, all samples exhibited an ≈2–4 nm thick stabilizer shell around the ZnO cores. The DLS results are shown in detail in Figure S2, Supporting Information.

To clarify whether the phase transfer is driven solely by the evaporation of cyclohexane, whilst the particles would otherwise remain dispersed in the organic solvent, the synthesis was carried out as a microwave-assisted, autoclave-like process. Thus, all solvents remained in the system, and both dispersion media were available to the particles. After performing the incubation in the microwave for 4 h, a two-phase system consisting of a turbid phase over an opalescent phase was obtained (see Figure S3, Supporting Information, for a photograph). The volumes corresponded to those of the solvents used, although traces of the other respective solvent are likely present in both phases and cause the observed turbidity or opalescence. The mainly aqueous opalescent phase—with an odor characteristic of cyclohexane—was removed from the vessel for SAXS analysis (see Figure S3, Supporting Information, for the data). Both before and after evaporation of the remaining cyclohexane, the scattering curve showed particles with the same radii as in the H_{240} particle system, but with a scattering intensity reduced by about 90%. During phase transfer in an open flask, about 50% of the water evaporates, though it remains in the system during microwave-assisted synthesis. The opalescence of the mainly aqueous phase could indicate the formation of a microemulsion in which the ZnO nanoparticles are locally dispersed in cyclohexane. An exclusively aqueous dispersion could then only be obtained by evaporation of the cyclohexane, whereby carrying out the phase transfer in an open vessel increases its efficiency by at least fivefold.

These results demonstrate that the described synthesis is suitable to obtain hydrophilic ZnO nanoparticles in an aqueous dispersion with tuneable particle size on the lower nanoscale. The observed growth process may be explained by coalescence, whereby up to $n_P = 16 \pm 1$ primary particles fuse during the heating phase to form the obtained larger particles. Niederberger et al. investigated kinetic and thermodynamic aspects of the microwave-assisted synthesis of ZnO nanoparticles in benzyl alcohol.[17] They found a particle growth according to the Lifshitz–Slyozov–Wagner model for coarsening, pointing to a diffusion-limited process. It is, in principle, possible that particle growth in our case follows that mechanism. But it is beyond the scope of the present work to provide evidence for such a mechanism.

2.2. Optical Properties

With the increasing size of semiconductor nanoparticles such as ZnO at the lower nanoscale, a complementary change in the optical properties is expected, as described earlier for the apolar ZnO particles used here.[5] **Figure 2** shows ultraviolet-visible (UV)-Vis and fluorescence spectra of the particles P_0 and H_{240}, i.e., before and after phase transfer, illustrating the redshift in both absorption edges and mean fluorescence energies. The former was determined employing Tauc plots, yielding bandgap energies of 3.44 ± 0.01 eV and 3.31 ± 0.01 eV for particles before and after phase transfer, respectively. The fluorescence spectra were approximated with Gaussian distributions, resulting in mean fluorescence energies of 2.20 ± 0.01 eV and 2.08 ± 0.01 eV with comparable full widths at half maximum of 0.63 ± 0.01 eV and 0.62 ± 0.01 eV, respectively. The exact cause of the optical properties of nanoscale ZnO, and thus its dependence on, e.g., stabilizing agents and the solvent, is still disputed, hence the analysis here is restricted to the determination of the respective energies.[18] The UV-Vis and fluorescence data support our interpretation from SAXS that the particles were grown in a defined way during the phase transfer.

2.3. Catalysis

A potential field of application for aqueous ZnO nanoparticle dispersions arises in photocatalysis. We have chosen MB as a model substance to test whether the particles H_{240} can photocatalytically decompose organic pollutants. MB has been frequently used to evaluate the photocatalytic activity of nanoparticles,[7,19,20] where the decomposition of the dye can be easily monitored with UV-Vis spectroscopy. We added H_{240} particles to a solution of

© 2021 The Authors. Advanced Engineering Materials published by Wiley-VCH GmbH

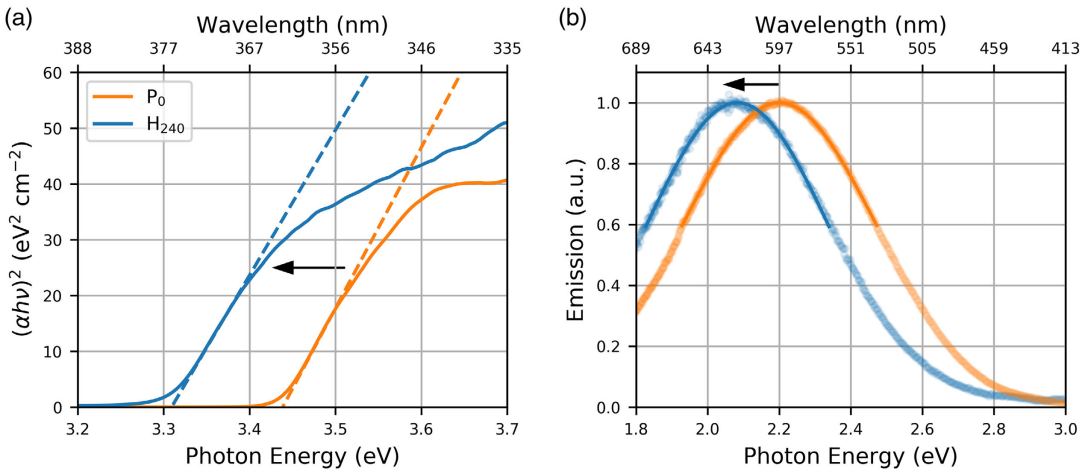

Figure 2. Normalized UV-Vis and fluorescence spectra of ZnO nanoparticles before (P_0) and after phase transfer (H_{240}). a) Tauc plot depicting the absorption edges (solid lines) and linear fits (dashed lines) for determination of the bandgap energies. b) Fluorescence data (symbols) and Gaussian fits (solid lines) for determination of the mean fluorescence energy.

MB and irradiated the solution with UV light with a wavelength of 365 nm. Over time, the solution discolored in the presence of H_{240}, while the color did not change substantially when no particles were added. This indicates that the H_{240} particles are photocatalytically active. Therefore, time-dependent UV-Vis spectra were measured to quantify the catalytic activity. A typical time series of the spectra is shown in panel a) of **Figure 3**. Two distinct absorbance bands are visible in the spectra with maxima at photon energies of $E = 1.8$ eV and 2.1 eV, respectively, corresponding to wavelengths of $\lambda = 689$ and 590 nm. For interpretation, we fitted each spectrum with the sum of two Gaussian functions f_1 and f_2 and a background contribution f_3. An example is depicted in panel b) of Figure 3, which corresponds to a reaction time of $t = 0$, i.e., directly after adding H_{240} to the solution of MB. It can be seen there that the measured spectrum (silver circles) is sufficiently well reproduced by the sum $f = f_1 + f_2 + f_3$ (blue, solid line). The individual contributions to the spectrum f_1, f_2, and f_3 are given for comparison (orange dashed line, green dash-dotted line, and red dotted line, respectively). The f_3 was modeled analogously to a scattering intensity I as a function of two constants a and b and the photon energy E as $I = a + b \cdot E^4$. Examples of the curves and curve fits are given in Figure S5, Supporting Information, for times of 0 and 1780 s after the start of the irradiation of the sample. Furthermore, the amplitudes A_1 and A_2 of f_1 and f_2 (left figure, second row), and the sum of both amplitudes ΣA (right figure, second row) are depicted. In the third row, plots of the time-dependent evolution of mean μ_1 and μ_2, and widths σ_1 and σ_2 of f_1 and f_2, are given, respectively. The last row shows the concentration of MB c_{MB} as a function of the irradiation time, and the decrease in ln c/c_0 with a linear fit, alongside its slope and intercept. The liner fit is interpreted in terms of a pseudo first-order reaction kinetics, expressed by

$$\ln \frac{c}{c_0} = -k_{app} \cdot t \tag{1}$$

Values for the apparent rate constants are $k_{app} = (0.222 \pm 0.010) \times 10^{-3}\,s^{-1}$ for H_{240} and $k_{app}(0.026 \pm 0.001) \times 10^{-3}\,s^{-1}$ for pure

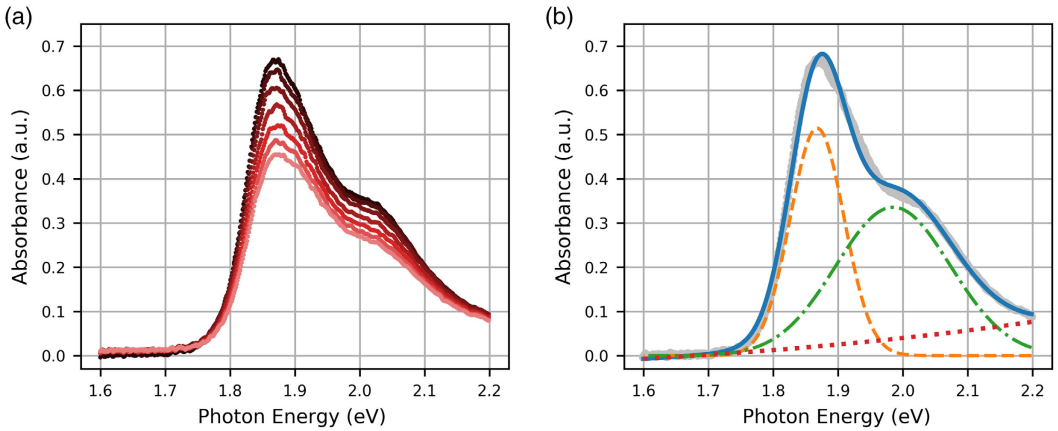

Figure 3. UV-Vis analysis of the photocatalytic degradation of MB employing H_{240} particles as catalyst. a) UV-Vis spectra taken in 300 s intervals, depicting the decrease of absorbance of the dye over time, and b) UV-Vis spectrum at a reaction time of 0 s (silver circles) and curve fit (blue, solid line) with the sum of two Gaussian functions f_1 and f_2 and a Rayleigh scattering contribution f_3 (orange dashed line, green dash-dotted line, and red dotted line, respectively).

© 2021 The Authors. Advanced Engineering Materials published by Wiley-VCH GmbH

water (Figure S6, Supporting Information). This means that the decomposition of the MB dye is increased by a factor of 8.5 in the presence of H_{240} in comparison to water as a control medium. Balcha et al. synthesized ZnO nanoparticles for photocatalysis.[21] They reported a maximum of $k_{app} = 12.4 \times 10^{-3}\,min^{-1}$, which is equivalent to 0.0207×10^{-3}, for a sol–gel prepared catalyst at a concentration of 250 mg L^{-1}. This value is close to that of H_{240}, where the catalyst concentration is much lower at 20 mg L^{-1}. After normalization of these values to the mass concentration of the particles, one could therefore assume that H_{240} has a much higher photocatalytic activity than the particles studied by Balcha et al.[21] Such a finding might be plausible due to the smaller size of H_{240} compared to the sol–gel synthesized particles, which have crystallite sizes of about 30 nm. However, caution is required in this interpretation.

Kisch and Bahnemann have laid out that the comparison of photocatalysts from different studies is intrinsically difficult.[22] One reason for this unsatisfactory situation is the difficulty to quantify the quantum yield correctly. Especially with semiconductor dispersions, a substantial part of the absorbance may be due to reflection and scattering and not absorption. Another issue arises from the use of polychromatic light sources, which complicates the determination of an apparent quantum yield. Further, the optical properties can differ substantially between different photoreactors, catalyst concentrations, and the reactions studied. To circumvent all these problems, to estimate the catalytic activity of H_{240}, we investigate commercially available ZnO and TiO_2 catalysts in the same conditions as H_{240}. In addition, a solution of a mixture of sodium oleate and polysorbate 80 was investigated to evaluate the influence of the stabilizer. All three samples were found catalytically active, and the data were evaluated in the same way as H_{240}, as shown in Figure S7–S9, Supporting Information. An overview of the decrease in the concentration of MB is given in **Figure 4**. Curve fits according to Equation (1) are given as straight lines and the k_{app} values are shown in panels a) and b) of Figure 4, respectively.

It can be seen that the commercial ZnO particles display the highest value of $k_{app} = (0.436 \pm 0.019) \times 10^{-3}\,s^{-1}$, closely followed by TiO_2 with $k_{app} = (0.412 \pm 0.020) \times 10^{-3}\,s^{-1}$. Noteworthy is that the stabilizer has a significant catalytic activity even without the presence of nanoparticles with $k_{app} = (0.104 \pm 0.004) \times 10^{-3}\,s^{-1}$.

As the ZnO nanoparticles of H_{240} are significantly smaller than those of the commercial ZnO particles, we expected that H_{240} also has a higher catalytic activity than the commercial ones. Nonetheless, this is not the case, and the observed, comparatively lower catalytic activity could be due to the stabilizer molecules on the particle surface. It is likely that polysorbate 80 renders the surface less accessible for MB as compared to the commercial samples without a stabilizer. The particle concentration of H_{240} of $cNP = 0.44 \pm 0.03 \times$ g L^{-1} and the volume-weighted surface area $VSSA_{NP} = (39 \pm 2) \times 10^3\,m^2\,m^{-3}$ were determined from the SAXS data. After dilution in the MB dye solution for investigation

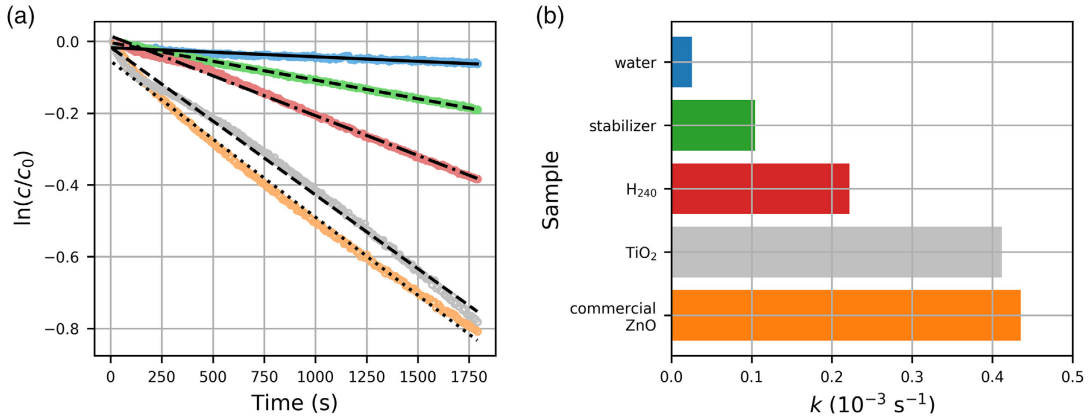

Figure 4. a) Plot of ln c/c_0 of MB dye as a function of irradiation time with UV light for pure water (blue), stabilizer (green), H_{240} (red), commercial ZnO (orange), and TiO_2 (silver), given in the order of increasing steepness of the decrease. Straight lines are linear fits for evaluation of the rate constants. b) Rate constants derived from the slopes of the curve fits in a).

Table 2. Parameters obtained from catalysis experiments on different samples: applied concentration of nanoparticles c_{NP}, resultant volume-weighted specific surface area $VSSA_{NP}$, determined apparent rate constant k_{app}, and normalised rate constants k_{app}/c_{NP} and $k_{app}/VSSA_{NP}$.

Sample	c_{NP} [mg L^{-1}]	$VSSA_{NP}$ 10^{-3} m^2	k_{app} $10^{-3}s^{-1}$	k_{app}/c_{NP} 10^{-3} L $g^{-1}s^{-1}$	$k_{app}/VSSA_{NP}$ $10^{-3}s^{-1}$ m^{-2}
This Synthesis					
ZnO particles (H_{240})	21 ± 1	3.9 ± 0.2	0.222 ± 0.010	11 ± 1	58 ± 4
Sodium oleate and polysorbate 80	–	–	0.104 ± 0.004	–	–
Blank (H_2O)	–	–	0.026 ± 0.001	–	–
Commercial particles					
25 nm ZnO	21 ± 1	1.9	0.436 ± 0.019	21 ± 2	232 ± 16
25 nm TiO_2	21 ± 1	2.5	0.412 ± 0.020	20 ± 2	165 ± 11

© 2021 The Authors. Advanced Engineering Materials published by Wiley-VCH GmbH

of the catalytic properties, the sample contained nanoparticles at a concentration of $21 \pm 1\,\mathrm{mg\,L^{-1}}$ and a surface area of $\mathrm{VSSA_{NP}} = (3.9 \pm 0.2) \times 10^{-3}\,\mathrm{m^2}$. The commercial comparison particles were then used at the same mass concentration, and the particle surface area available in each case was calculated based on the particle size specified by the manufacturer. The determined values for k_{app} with nanoparticle concentration- and surface area-normalized values k_{app}/c_{NP} and $k_{app}/\mathrm{VSSA_{NP}}$ are listed in **Table 2**. The surface-normalized rate constants of $(58 \pm 1) \times 10^{-3}\,\mathrm{s^{-1}\,m^{-2}}$ (H_{240}), $(232 \pm 16) \times 10^{-3}\,\mathrm{s^{-1}\,m^{-2}}$ (commercial ZnO), and $(165 \pm 11) \times 10^{-3}\mathrm{s^{-1}\,m^{-2}}$ quantify the differences in the catalytic activity.

3. Conclusion

Hydrophobic oleate-coated ZnO nanoparticles with a mean radius of $R_{mean} = 2.3 \pm 0.1$ nm were prepared by an established microwave-assisted synthesis and obtained in cyclohexane.[5] To transfer these ultrasmall nanoparticles to an aqueous medium, they were coated with polysorbate 80, and the organic solvent was removed after the addition of water under low pressure. To obtain aggregate-free particle systems, an intermediate heating process at 90 °C was needed, the duration of which determined the final particle size. Thus, hydrophilic ZnO nanoparticles with sizes between $R_{mean} = 3.7 \pm 0.1$ nm and $R_{mean} = 5.7 \pm 0.1$ nm in aqueous dispersion were obtained. These particles could be utilized in photocatalysis, which was demonstrated by the degradation of MB.

4. Experimental Section

Materials: All chemicals were used as received without further purification. Sodium oleate (95%) was purchased from abcr, zinc(II) chloride and Polysorbate 80 from Merck, and tetrabutylammonium hydroxide (1 M in methanol) from Sigma-Aldrich. Cyclohexane, ethanol, and tetrahydrofuran were purchased from Th. Geyer. Ultrapure water (Milli-Q, 18.2 Ω cm at 25 °C) was used.

Nanoparticle Synthesis: Hydrophobic, oleate-coated ZnO nanoparticles were obtained as described previously.[5] Briefly, 166 mg (264 µmol) zinc oleate was dissolved in 4.736 mL tetrahydrofuran, and after the addition of 264 µL of 1 M tetrabutylammonium hydroxide in methanol, the microwave-assisted synthesis of particles was carried out at 125 °C for 5 min. Particle purification was carried out by two times precipitation in a fourfold excess of ethanol and subsequent dispersion in cyclohexane.

Phase Transfer: A volume of 3.5 mL particle dispersion ($1.8 \pm 0.1 \times$ g $\mathrm{L^{-1}}$ ZnO in cyclohexane) was used for the phase transfer of the particles from cyclohexane to water. An amount of 50 µL polysorbate 80 (53 µg, 40 µmol) was added to the dispersion and stirred for 10 min. Then, 10 mL of water was added and stirred for another 10 min at a temperature of 21 °C. Afterward, the temperature was set to 90 °C for time intervals of 0, 15, 30, 60, 90, and 240 min. The cyclohexane was completely removed after a heating time of 240 min, as indicated by the absence of its characteristic smell. The reaction vessel (round flask with a volume of 50 mL) remained open during phase transfer. A volume of 5 mL of water evaporated during the experiment, which was replaced at the end of the experiment. Therefore, the amount of polysorbate 80 in the aqueous particle suspension was 5 mL per liter. A rotary evaporator was employed to remove the remaining cyclohexane from the samples obtained at shorter heating times at a pressure of 100 mbar and a temperature of 40 °C. The obtained aqueous particle dispersions were centrifuged for 20 min (H_{15}: 90 min) at 12 000 × g to remove any aggregates. All particles were stable for 7 days. After this period, the particles start to aggregate and form sediment.

Catalysis Experiment: The catalytic performance of the phase-transferred particles was analyzed by the photocatalytic degradation of MB as a 10^{-5} M solution in water. An aqueous solution containing 1 vol% polysorbate 80 and $22.4 \times$ g $\mathrm{L^{-1}}$ sodium oleate was prepared as a reference sample. Samples used were an aqueous solution containing $21 \times$ g $\mathrm{L^{-1}}$ particles, the reference sample, or water. A volume of 100 µL of the sample solutions was added to 2 mL of the MB solution contained in a 10 × 10 mm High Precision Quartz Cell from Hellma Analytics under stirring. The samples were irradiated using a Herolab UV-4 S $\mathrm{L^{-1}}$ hand lamp at an indicated wavelength of 365 nm and UV-Vis spectra were recorded using a StellarNet Inc. BLACK-Comet C-50 Spectrometer with an SL5 Deuterium + Halogen Light Source and a DP400 dip probe with 10 mm optical path length. For the photocatalysis experiment, particles were added to a solution of MB dye so that the final catalyst concentration was 21 ± 1 mg $\mathrm{L^{-1}}$. This sample was placed in a quartz cuvette and, under UV irradiation with a wavelength of 365 nm, the change in MB absorbance was monitored in 10 s intervals for 30 min. A sketch of the experimental setup can be found in Figure S4, Supporting Information, and based on the geometries of the UV lamp and the cuvette, the photon flux hitting the sample was estimated at around $1.9 \times 10^{15}\,\mathrm{s^{-1}}$.

SAXS Measurements: SAXS measurements were performed in a polycarbonate flow-through capillary at 21 ± 1 °C with a SAXSess instrument (Anton Paar, Austria) attached to a laboratory X-ray generator (PW3830, PANalytical) and operated with a fine focus glass X-ray tube at a voltage of 40 kV and a current of 40 mA (Cu Kα, $\lambda = 0.1542$ nm). Focusing multilayer optics and a block collimator provide a monochromatic primary beam with low background noise. SASfit version 0.94.11 was used for curve fitting and the determination of the particle size distribution.[14]

DLS Measurements: DLS measurements were performed using a multiangle ALV 7004 device with a He-Ne-Laser ($\lambda = 632.8$ nm) from ALV Langen. The samples were used as obtained from the phase transfer procedure without dilution or filtration. Data evaluation was performed according to the ISO standard 13321:1996 and with the CONTIN program by Provencher to obtain the hydrodynamic radii R_H.[23]

UV-Vis Measurements: UV-Vis measurements were performed using a StellarNet Inc. BLACK-Comet C-50 Spectrometer with an SL5 Deuterium + Halogen Light Source. Aqueous dispersions were used as prepared, whilst dispersions in cyclohexane were diluted in a ratio of 1:20, and then filled into a 10 × 10 mm High Precision Quartz Cell from Hellma Analytics. A Tauc plot was used to determine the optical absorption edges.

Fluorescence Measurements: Fluorescence measurements were carried out on a HORIBA Fluorolog-3 spectrofluorimeter. The particle systems were prepared in the same way as for UV-Vis measurements. Excitation wavelengths 10 nm smaller than the absorption edges, as determined by UV-Vis measurements, were chosen, and Gaussian approximations were employed to determine the mean fluorescence energy.

Supporting Information

Supporting Information is available from the Wiley Online Library or from the author.

Acknowledgements

The authors thank Frederik Firschke for experimental assistance, V.-D. Hodoroaba and S. Benemann for the electron microscopy image, Thomas Risse for valuable discussions, and Glen J. Smales for proofreading the manuscript.

Open access funding enabled and organized by Projekt DEAL.

Conflict of Interest

The authors declare no conflict of interest.

© 2021 The Authors. Advanced Engineering Materials published by Wiley-VCH GmbH

Data Availability Statement

Research data are not shared.

Keywords

nanoparticles, SAXS, zinc oxide

Received: September 20, 2021
Revised: November 6, 2021
Published online: December 2, 2021

[1] A. Kolodziejczak-Radzimska, T. Jesionowski, *Materials* **2014**, *7*, 2833.
[2] S. G. Kumar, K. Rao, *RSC Adv.* **2015**, *5*, 3306.
[3] Y. Kumar, S. Tayyab, S. Muzammil, *Arch. Biochem. Biophys.* **2004**, *426*, 3.
[4] B. O. Bica, J. V. S. de Melo, *Constr. Build Mater.* **2020**, *252*, 119120.
[5] P. E. J. Saloga, A. F. Thünemann, *Langmuir* **2019**, *35*, 12469.
[6] Z. L. Wang, *J. Phys.: Condens. Matter* **2004**, *16*, R829.
[7] A. Houas, *Appl. Catal., B* **2001**, *31*, 145.
[8] A. Syed, Z. Z. Wang, I. Zhitomirsky, *Mater. Lett.* **2019**, *252*, 165.
[9] J. Milne, R. M. E. Silva, Z. Z. Wang, I. Zhitomirsky, *Ceram. Int.* **2019**, *45*, 2498.
[10] R. Borah, R. Ninakanti, G. Nuyts, H. Peeters, A. Pedrazo-Tardajos, S. Nuti, C. Vande Velde, K. De Wael, S. Lenaerts, S. Bals, S. W. Verbruggen, *Chem. – Eur. J.* **2021**, *27*, 9011.
[11] L. S. Schwartzberg, R. M. Navari, *Adv. Ther.* **2018**, *35*, 754.
[12] W. Ren, G. Tian, S. Jian, Z. Gu, L. Zhou, L. Yan, S. Jin, W. Yin, Y. Zhao, *RSC Adv.* **2012**, *2*, 7037.
[13] B. R. Pauw, C. Kästner, A. F. Thünemann, *J. Appl. Crystallogr.* **2017**, *50*, 1280.
[14] I. Breßler, J. Kohlbrecher, A. F. Thünemann, *J. Appl. Crystallogr.* **2015**, *48*, 1587.
[15] B. L. Caetano, V. Briois, S. H. Pulcinelli, F. Meneau, C. V. Santilli, *J. Phys. Chem. C* **2017**, *121*, 886.
[16] A. Amani, P. York, H. de Waard, J. Anwar, *Soft Matter* **2011**, *7*, 2900.
[17] I. Bilecka, P. Elser, M. Niederberger, *ACS Nano* **2009**, *3*, 467.
[18] A. Janotti, C. G. Van de Walle, *Rep. Prog. Phys.* **2009**, *72*, 126501.
[19] R. Asahi, *Science* **2001**, *293*, 269.
[20] A. Mishra, A. Panigrahi, P. Mal, S. Penta, G. Padmaja, G. Bera, P. Das, P. Rambabu, G. R. Turpu, *J. Alloys Compd.* **2020**, *842*, 155746.
[21] A. Balcha, O. P. Yadav, T. Dey, *Environ. Sci. Pollut. Res.* **2016**, *23*, 25485.
[22] H. Kisch, D. Bahnemann, *J. Phys. Chem. Lett.* **2015**, *6*, 1907.
[23] S. W. Provencher, *Comput. Phys. Commun.* **1982**, *27*, 229.

© 2021 The Authors. Advanced Engineering Materials published by Wiley-VCH GmbH